Journal of Magnetic Resonance 319 (2020) 106800

Contents lists available at ScienceDirect

Journal of Magnetic Resonance

journal homepage: www.elsevier.com/locate/jmr

Low-cost low-field NMR and MRI: Instrumentation and applications

Carl A. Michal

Department of Physics and Astronomy, University of British Columbia, 6224 Agricultural Road, Vancouver, BC V6T 1Z1, Canada

ARTICLE INFO

Article history:
Received 30 June 2020
Revised 25 July 2020
Accepted 26 July 2020

Keywords:
Software-defined radio
FPGA
Microcontroller
Arduino
Inhomogeneous magnetization transfer
Two-photon excitation

ABSTRACT

While NMR and MRI are often thought of as expensive techniques requiring large institutional investment, opportunities for low-cost, low-field NMR and MRI abound. We discuss a number of approaches to performing magnetic resonance experiments with inexpensive, easy to find or build components, aimed at applications in industry, education, and research. Opportunities that aim to make NMR accessible to a broad community are highlighted. We describe and demonstrate some projects from our laboratory, including a new prototype instrument for measurements at frequencies up to ~200 kHz and demonstrate its application to the study of the rapidly advancing technique known as inhomogeneous magnetization transfer imaging, a promising method for characterizing myelin in vivo.

1. Introduction

Despite its reputation as an expensive and insensitive technique, observation of NMR as a physical phenomenon, and its use in a number of applications, can be accomplished with very modest instrumentation. In fact both NMR and MRI can be performed with surprising ease at extraordinarily low cost. In comparison to state-of-the art high-field NMR and MRI, where instrument costs are measured in the millions, low-cost NMR might mean $50,000 for a commercial instrument or $200 for a home-built DIY project. A renaissance in recent years of hobby-oriented electronic components and microcontrollers has put surprisingly powerful NMR and MRI within the reach of anyone with a tiny budget and some basic electronics and mechanical skills. While these low-cost DIY efforts are not likely to compete with the state-of-the art from the full-service instrument vendors in many scenarios, there is a surprising range of applications available, and considerable science that can be done, with inexpensive hardware.

In this perspective, we discuss a number of approaches to performing NMR experiments with inexpensive, easy to find or build components, highlighting a number of projects that aim to make NMR accessible to a broad community. We introduce some of the design considerations of low-field instrumentation, and describe and demonstrate some projects from our laboratory, including an early prototype instrument assembled at home during the spring of 2020 COVID-19 lock-down. Examples of applications for these kinds of low-cost systems include education, fundamental NMR physics including two-photon excitation, study of J couplings, and magnetization transfer experiments relevant to in vivo brain imaging. Opportunities at an ultra-low-cost hobbyist/DIY level are emphasized.

2. Design considerations

We begin with an introduction to some of the design considerations pertinent to low-cost NMR systems. The goal is not to provide a comprehensive tutorial on instrument design, rather we aim to present a brief discussion of some of the most important issues and provide links to resources.

2.1. Sensitivity & coil design

Arguably the most important consideration in the design of any NMR system is sensitivity. The voltage signal induced in a coil by a sample containing nuclear spins with their magnetization initially aligned perpendicular to the static magnetic field can be straightforwardly calculated using the principle of reciprocity [1,2] and can be expressed as

$$V_{\text{signal}} = \int \left(\frac{B_1}{i_1}(r)\right) \omega_0 M_0 \, dV, \tag{1}$$

where $B_1(r)/i_1$ is the field that would be produced at position r by a unit current in the receive coil, ω_0 is the Larmor frequency, the integral is over the sample volume, and M_0 is the sample magnetization, given by

E-mail address: michal@phas.ubc.ca

https://doi.org/10.1016/j.jmr.2020.106800
1090-7807/

$$M_0 = \frac{N_s \gamma^2 \hbar^2 I(I+1) B_p}{3 k_B T}. \quad (2)$$

N_s is the density of nuclear spins, having gyromagnetic ratio γ and spin I, in the sample, B_p is the strength of the magnetic field in which they are polarized, k_B is the Boltzmann constant, $\hbar$ is the Plank constant divided by 2π, and T the sample temperature. If the sample is polarized in the same magnetic field that is used for detection, then $\gamma B_p = \omega_0$. The quantities in Eqs. (1) and (2) are all relatively straightforward to work with, and at low field satisfying agreement can be found with expectations from introductory electricity and magnetism theory, for example calculation of B_1/i_1 using the Biot-Savart law is sufficient at low frequency. Substantial deviations from the predictions of such idealized approaches may be observed if, for example the receive coil is strongly coupled to another coil.

The noise in an inductively detected NMR experiment is limited by the Johnson noise associated with the resistance of the receive coil windings, and is given by

$$V_{\text{Johnson}} = \sqrt{4 k_B T \Delta f R}, \quad (3)$$

where Δf is the bandwidth of the measurement and R is the coil's resistance at ω_0. It is important to note that even at low frequency, R may be much greater than the DC resistance due to both the skin and proximity effects [2]. The relevant resistance is most easily found from the quality factor, Q, of a resonant circuit based on the coil using $Q = \omega L/R$ where L is the coil's inductance and ω is the circuit's resonance frequency. From Eqs. (1)–(3), the signal-to-noise ratio of an idealized NMR experiment in the time domain can be calculated. Both the signal and noise voltages are multiplied by a factor Q if the coil is incorporated into a resonant circuit.

In practice, achieving signal to noise ratios approaching those predicted by the equations above depends on both careful preservation of the signals collected from the receiver coil and the exclusion of introduced noise from other sources. Noise is easily introduced from the environment directly into the receive coil or to the receiver circuitry. In addition, the receiver circuitry itself must be designed so that noise associated with the receiver components does not dominate over the coil's Johnson noise. Suitable low-noise preamplifiers are now widely available. Low-noise amplifiers at rf frequencies are available for example from Minicircuits (http://www.minicircuits.com) and from numerous vendors in online "maker" marketplaces (e.g. aliexpress.com, dx.com, etc.). At lower frequencies, op-amps or instrumentation amplifiers available from numerous electronics parts vendors will suffice. Such amplifiers must be selected with care however, taking into account both the frequency and source impedance of the receive circuit. Some vendors produce useful design notes that aid in part selection for optimal signal-to-noise ratio (SNR) [3,4].

Two common strategies for eliminating environmental noise pickup by the receive coil are shielding and differential coil design. Shielding is simple and straightforward, but at low frequency can require a large amount of metal. Copper makes an excellent shield, though it is heavy and expensive. Aluminum is a more common choice, but requires thicker shields. A key parameter in designing or evaluating a shield is the skin depth, which is given by

$$\delta = \sqrt{\frac{2}{\omega \mu \sigma}} \quad (4)$$

in which μ is the permeability of the material and σ is its conductivity. While it is widely thought that the thickness required for a useful shield depends only on the ratio of the shield thickness to the skin depth, a shield will begin to have effects if its thickness satisfies $rt \gtrsim \delta^2$, where t is the shield's thickness and r is the radius of the path of the eddy currents responsible for the shielding [5]. For a cylindrical shield with its axis parallel to the receive coil axis, r is the radius of the shield. In the thin shield regime, where $t \lesssim \delta$, the field inside the shield is attenuated by a factor $1/\sqrt{1 + (rt/\delta^2)^2}$. For shields thicker than the skin depth, the thickness dependence is given approximately by $2\sqrt{2}\delta \exp(-t/\delta)/r$, and is typically much better than would be expected based on the exponential factor alone. A full treatment can be found in Ref. [6]. For aluminum at 2 kHz, $\delta \approx 2$ mm, and we have had much success by placing the receive coil inside a section of 150 mm diameter, 7 mm wall aluminum pipe with the ends left open. An iron or steel shield could be much thinner, but due to the magnetic properties, these materials perturb the local field and are likely to dramatically reduce the homogeneity of the magnetic field. Shielding the receiver electronics from noise pickup, if necessary, can however be accomplished with a thin steel enclosure, as long as it is placed sufficiently far from the sample to not disturb the magnetic field.

Differential or gradiometric coil design makes use of multiple coil segments arranged in opposition so that the pick-up from environmental noise is cancelled while the signal is not. While this strategy has been implemented in various ways, perhaps the most efficient approach is one where two opposing symmetric coil segments are both used to collect NMR signals from different sample volumes, as used for example in the design of a large-scale Earth's field NMR system [7].

It can be seen from Eq. (3) that the thermal noise due to the receive coil's resistance scales with the square root of the resistance. The SNR can thus be improved by reducing this resistance. Copper is almost universally chosen for such coils. For a solenoidal coil, the questions then arise: what wire size to use and how many turns? At very low frequency, where the proximity effect and skin effect are negligible, the SNR calculated from Eqs. (1) and (3) scales simply so that it depends on the total mass of copper wire used. As an example, a single-layer 100 turn coil of 1 mm diameter wire would be expected to give identical SNR to that of a two-layer 400 turn coil of 0.5 mm diameter wire as both coils use the same amount of copper. The smaller wire would have four times the resistance per unit length as the larger, and would need to be four times longer, giving a coil with 16 times the resistance of the coil with the larger diameter. The Johnson noise from the coil would be $\sqrt{16}$ or four times larger, but the signal from the nuclear spins would also be four times larger due to the greater number of windings. Certainly winding a coil with fewer turns is simpler, but a number of other considerations influence the decision. A larger number of windings has the advantage of making both the signal and noise voltages larger, easing the noise performance requirements of the receiver amplifier. As the number of windings is increased however, the proximity effect, which amounts to an increased resistance due to redistribution of ac currents in a conductor in response to the magnetic fields produced by nearby currents [1], becomes increasingly important. This results in a greater resistance than would be expected based on the wire dimensions alone, and increases in importance for greater winding density. For higher frequencies the skin effect, which limits the current flow to the outer layer of a conductor, will also be important. This effect increases the wire's resistance by effectively limiting the useful volume of conductor to the surface layer. As Eq. (4) shows, the skin-depth scales with the square root of the frequency. At 2 kHz it is approximately 1.5 mm in copper so that its effects are minimal for typical wire sizes, but along with the proximity effect it plays a significant role at higher frequencies.

In addition, capacitance between the coil windings results in the coil having a self-resonance frequency, above which the coil is not useful in a resonant circuit. The self-capacitance and proximity effects limit the number of turns that can be used in a practical coil. Consequences of the skin and proximity effects at modest fre-

quencies can be reduced with the use of Litz wire, consisting of multiple braided filaments, and self-capacitance can be reduced by winding coils in sections [8]. One can get surprisingly far in understanding instrument performance at frequencies as high as 100's of kHz with low-frequency electromagnetism (e.g. Biot-Savart law) as long as one is willing to work below a coil's self-resonance frequency and remember that the coil's effective resistance is strongly frequency and geometry dependent.

2.2. The magnet

One of the most significant costs in many NMR set-ups is a magnet supplying a stable, uniform magnetic field. For low-field NMR, a number of magnet options are possible, including those based upon electromagnets, permanent magnets, and the Earth's geomagnetic field.

Many low-cost NMR systems rely on the Earth's magnetic field, as it comes essentially for free. Locally, the Earth's field tends to be both very uniform and reasonably stable on the time-scale of most NMR experiments, although temporal fluctuations can be important in some applications (e.g. [9]) and might even be the target of the measurement [10]. Depending on the environment, the local field can be significantly disturbed in amplitude, direction, and homogeneity by objects surprisingly distant from the experiment. The effects of fluctuations can be mitigated by a number of strategies, for example the use a second spectrometer as a sensitive field sensor to provide either a reference frequency for demodulating the signals of interest [9] or as part of a field-frequency lock. Use of the Earth's field comes with a number of challenges, in particular the low frequency precludes the observation of chemical shifts, and the low field makes sensitivity a challenge, due both to the low nuclear spin polarization at thermal equilibrium and the small signals that are induced at low frequency. Some of these challenges can be overcome with non-thermal polarization, for example by pre-polarizing in a stronger magnetic field, using an optically pumped noble gas [11], using dynamic nuclear polarization with free radicals [12], or SABRE (signal amplification by reversible exchange) [13].

The availability of strong, stable rare-earth magnets has made NMR and MRI with permanent magnets feasible. A number of vendors now produce systems spanning the range from bench-top NMR to human MRI based on permanent magnets. To produce a stable enough magnetic field for high-resolution, the temperature of the magnet components must be carefully controlled. Producing a homogeneous magnetic field with permanent magnets requires considerable expertise, though many NMR measurements can be performed in very inhomogeneous fields. Permanent magnet-based instruments allow a wide range of NMR methodologies and have been reviewed recently [14]. The development of small-scale magnets is an area of continued active research [15]. With careful selection of elements, precision construction, and active shimming, extremely high resolution can be achieved allowing bench-top NMR spectrometers with spectral linewidths competitive with high-resolution NMR in superconducting magnets.

Electromagnets are perhaps the most flexible option. Solenoids and Helmoltz pairs are simple to construct and can be improved to enlarge the uniform regions within [16,17] Many other designs are possible, and even coils adequate for in vivo imaging can be wound straightforwardly with relatively simple design [18].

2.3. Console electronics

The sophistication of the electronics needed to run an NMR experiment varies dramatically with the complexity and scale of the experiment. In recent years it has become possible to construct the transmit, receive, and control electronics needed for even very advanced experiments inexpensively. The widespread availability of powerful microcontrollers, field-programmable gate arrays, and software-defined radio devices has made event control and coherent signal generation on the timescales needed for NMR and MRI to be within reach of widely available inexpensive devices. A variety of examples will be discussed further below.

3. Examples and applications

3.1. Free precession

Probably the simplest method of observing a free induction decay is with the free precession method of Packard and Varian [19]. In this experiment, the nuclear spins in a sample, typically water, are polarized with a magnetic field due to an electromagnet aligned perpendicular to the Earth's magnetic field. This pre-polarization field is turned off rapidly enough that the magnetization is left perpendicular to the Earth's field, and then precesses around it. A free-induction decay may be observed in a suitably aligned coil, which could in fact be the same coil used to provide the polarization field. The magnet providing the polarization field need not meet any homogeneity requirement and so can be crudely wound by hand without seriously compromising the instrument's performance. If care is taken in the siting of the system and selection of materials used in construction, the homogeneity of the Earth's field allows for a long free-induction decay and sharp, relatively easily observed signals. Due to its simplicity, this method has been widely implemented, and provides an elegant way of observing signals from nuclear spins. A number of projects and publications have made designs for this style of instrument available to a skilled hobbyist or student.

One example of such a project is the "how-to" book, "Signals from the Subatomic World: How to Build a Proton Precession Magnetometer" [20], which provides detailed step-by-step instructions and plans for the Magnum-1, an instrument intended to provide a sensitive measure of the local magnetic field strength. A second example is an open-hardware/software instrument, called pyPPM [21] which similarly provides complete plans, software, and parts lists. Drawings and representative data from the pyPPM project are shown in Fig. 1.

Different design choices were made for these two instruments. The pyPPM uses a single coil assembly for polarization and signal detection while the Magnum-1 has separate polarization and receive coils, each optimized for their function. The Magnum-1 uses a differential coil design, with two coil segments wired so as to cancel pick-up of environmental noise, while the first generation pyPPM does not. Both systems are controlled with inexpensive microcontollers, supplied with firmware, and are controlled through serial connections to personal computers.

Systems like these have been used as magnetic field monitors for geophysical studies [10] and even, with DNP, on satellites [22], but this style of instrument can also be used to make T_1 relaxation measurements, observe J-couplings, and could be used to do rudimentary imaging. These features make this style of instrument an excellent teaching tool, and in fact a commercial instrument designed for this purpose exists [23]. One other interesting application of an Earth's field precession system is a "maker" project to explore imaging in inhomogeneous fields using code coils rather than linear gradients in analogy to coded-aperature spectroscopy [24].

These instruments however, all lack the ability to manipulate the nuclear spin magnetization after the polarization coil has been turned off, limiting the range of experiments available.

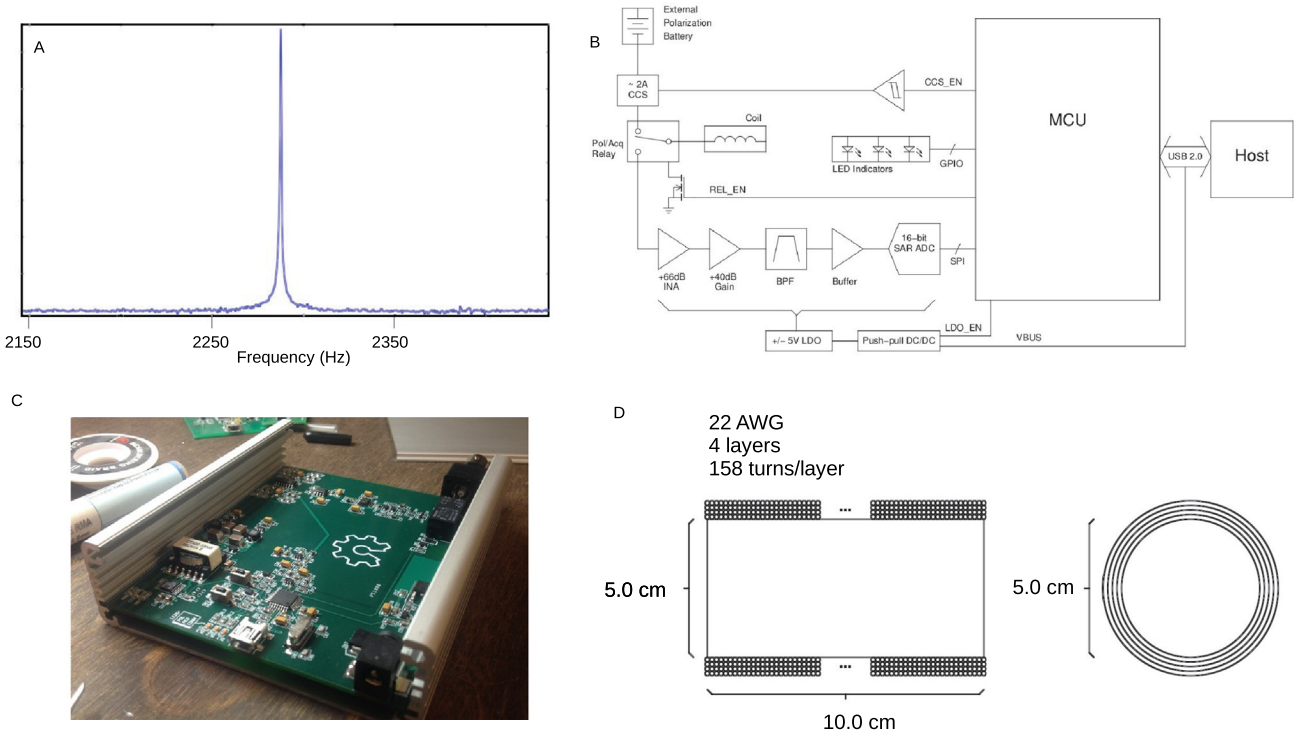

Fig. 1. The pyPPM project. (A) shows an Earth's field NMR spectrum of water following the rapid shut-off of a strong polarization field. A block diagram of the pyPPM spectrometer system is shown in (B). (C) shows a completed pyPPM circuit board and the coil design is shown in (D). Images from the pyPPM project [21] courtesy Bradley Worley, used with permission.

3.2. Earth's field pulsed spectrometers

A much wider variety of experiments can be performed with a pulsed spectrometer. A number of pulsed Earth's field NMR systems have been described, many early works were reviewed by Béné [25]. More recent systems include an apparatus for imaging in the Earth's field [26], one used to study diffusion in Antarctic sea ice brine [27], and one used to demonstrate the feasibility of chemical analysis with Earth's field instrumentation [28]. These systems all rely on prepolarization to make signals observable in the Earth's field. While the pre-polarization field must be extinguished rapidly in the free precession systems described above, for systems with pulsed excitation, there is additional flexibility in the pre-polarization arrangement. If the pre-polarizing field is oriented along the Earth's field, the shut-off need only be rapid enough compared to T_1 that the nuclear spin polarization is not lost during the shut-off. If the pre-polarization field is orthogonal to the Earth's field, or indeed in different directions in different parts of the sample, as in [29], then as the strength of the field is reduced to a value similar to the Earth's field, the shut-off must be slow enough to be adiabatic. This adiabatic shut-off rotates the polarization to lie along the Earth's field, after which conventional pulsed NMR experiments can be performed.

The pyPPM project version 2 [21] aims to be a complete pulsed NMR spectrometer, incorporating pre-polarization, computer controlled coil tuning, and shim gradients. Complete schematics and design files have been published under an open-source license.

Callaghan et al.'s system, designed for use in Antarctica [27], provides an excellent starting point for the low-cost instrument builder, as complete schematics for the pre-polarization and amplifier circuits along with some discussion of design rationale are provided, along with full descriptions of the coils. However, for pulse control and digitization a commercial NMR spectrometer console was used, making the system as a whole decidedly a laboratory instrument. The capabilities required of this commercial console however can now be found on inexpensive microcontroller platforms which can be used to both generate pulses and control other components such as switches, relays and power supplies. On-board ADCs are sufficient to digitize the received signals. A system based on Callaghan's design, but with updated parts, simplified circuit designs, and the expensive commercial console replaced with an arduino Uno microcontroller has been described in detail [30]. This system was designed for use as a low cost educational tool, and is simple enough to build that it has been reproduced numerous times by students and hobbyists. A diagram of the apparatus is shown in Fig. 2. The most challenging component of this system to build is the transmit/receive coil, which has 3000 turns of wire, and is tedious, but not impossible, to wind by hand. In contrast to the free precession systems, the receive coil of this system, following Callaghan's design, is a multilayer coil that does not reject environmental noise. Instead, the coil is shielded, in part by the polarization coil which is shorted while signals are collected, but also by placing it inside a thick (7 mm) aluminum shield. The system's capabilities were extended with the addition of three gradient coils and a field coil, constructed from copper foil tape on mylar sheets which were then wrapped on the aluminum shield, in order to facilitate shimming and simple imaging experiments [31]. The field coil allows the resonance frequency to be shifted away from noise appearing at fixed frequencies, typically odd-harmonics of the 60 Hz power-line. With the three simple gradient coils the magnetic field can typically be shimmed to better than 1 Hz fwhm indoors as long as the coil assembly is placed sufficiently far (about 1 m) from furniture and building materials. A representative image of a 500 ml water bottle containing a plastic + shape is shown in Fig. 2. These systems were designed as teaching tools to explore electromagnetism in an introductory physics course.

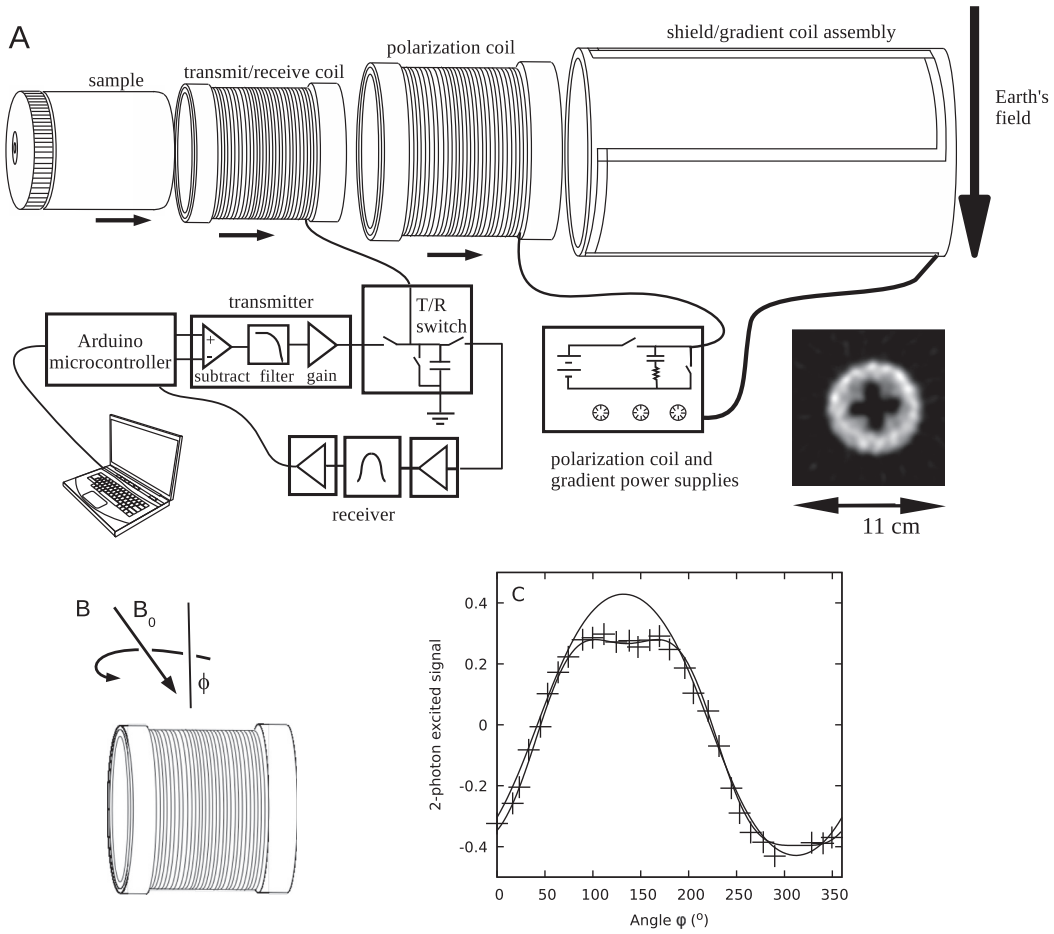

Fig. 2. Low-cost pulsed Earth's field NMR. (A) Block diagram of the arduino Uno based system. The transmitter and receiver each consist of three op-amps. The polarization coil current is provided from a computer power supply. The addition of gradient coils allows imaging; a representative image of a 500 ml water bottle with an extruded plastic + shape is shown in the inset. Complete schematics of all the components are supplied in [30]. (B) and (C) Two-photon excitation NMR experiments performed with this Earth's field instrument. The coil assembly is rotated about the horizontal axis, as shown in (B) and the resulting signal appearing in the coil is shown in C. (A) is reprinted from Ref. [31], used with permission.

Beyond educational purposes, our Earth's Field NMR system has been used to study non-linear effects in NMR. While the Bloch-Siegert shift is well known, less appreciated is the fact that NMR signals can be excited by excitation at one-half (and other sub-multiples) of the Larmor frequency. Early investigations of both of these nonlinear phenomena were made in the Earth's field [32], where their relative size, which scales with B_1/B_0, can be made very large. From a quantum-mechanical perspective, multi-photon excitation can be thought of as requiring two or more rf photons whose energy and angular momentum add to span a transition. For two-photon excitation, this requires one rf component to lie along the static magnetic field, B_0 [33]. The dependence of the NMR signal following a constant duration half-frequency excitation pulse on the orientation of the transmit/receive coil in our Earth's field apparatus is shown in Fig. 2C. The coil is rotated about the vertical axis as indicated. On-resonance excitation has only a weak dependence on this orientation as the Earth's field lies $\sim 67^\circ$ below the horizontal axis. The two-photon excited signal however changes sign as the orientation is varied because the component of B_1 *parallel* to B_0 changes sign as the coil is rotated, changing the sign of the effective B_1. With leading order effects only, as would be expected if B_1/B_0 was small, the expected pattern is roughly sinuisoidal, but when B_1/B_0 is not small, a more complicated dependence is observed. A direct simulation of the Bloch equations provides an excellent fit to the data, shown as the solid line.

3.3. Beyond Earth's field

While systems acquiring signals in the Earth's field have the advantage of a stable, uniform resonance frequency, and methodological and instrumentation developments continue to expand the range of applications possible (e.g. [34]), sensitivity is a significant limitation. At higher field strengths a much greater variety of applications and experiments are possible. Simple electromagnets with modest power supplies can be used to make low fields in the mT range while permanent magnets can create much stronger fields.

One example application is the development of embedded environmental sensors. Small NdFeB disk magnets were used with planar rf coils to make unilateral NMR sensors, that were then encased in epoxy and embedded in concrete to monitor curing and drying processes [35]. The entire magnet and rf sensor assembly is a 30 mm diameter, 12 mm tall cylinder with a field of 0.24 T. Unilateral NMR systems like this have found diverse applications [36] ranging from art conservation [37,38] to evaluating food spoilage [39]. Another embedded sensor project aimed to monitor the clogging of gravel filter beds for wastewater treatment in wetlands [40]. There, pairs of disk magnets were assembled in analogy to Helmoltz coils and provided a field > 0.3 T. These kinds of projects exemplify the argument made recently [41] that widespread use of magnetic resonance technology and a blossoming of applications will come with low-cost, low-field instrumentation. In that work,

a small, portable, unilateral NMR magnet and probe design, shown in Fig. 3 was demonstrated. The system was compared to a single-voxel imaging system, and the signals arise from a sensitive volume which takes the form of a 2-mm diameter sphere about 5 mm above the magnet surface. Objects can be scanned over the sensor, or vice versa, to allow spatially depedent measurement of hydrogen content, relaxation times and diffusion coefficients. While the homogeneity of permanent magnet systems varies, and construction of systems suitable for high-resolution spectroscopy remains challenging, these examples demonstrate that very simple, inexpensive magnet systems can be constructed to use NMR for a wide range of applications.

Modern permanent magnets have also made high quality imaging systems possible. An impressive low-cost MRI system has recently been developed for educational and prototyping purposes [42]. This system allows conventional Fourier imaging and can image samples up to 2 cm in diameter. Drawings, schematics and software for this device have been provided to allow its reproduction. The system uses an H-shape dipole yoked magnet design, shown in Fig. 4 along with representative images of both phantoms and mouse brain. The console used is the MEDUSA design, which is controlled from a personal computer over USB [43] and provides a configurable number of digital rf and gradient channels. The real-time control is provided by an FPGA logic core, the digital rf uses chips from Analog Devices Inc., AD9854 synthesizers and the AD6620 digital receiver, the latter first applied to NMR in Ref. [44].

A permanent magnet system has been designed for in vivo pediatric imaging [45], and is shown in Fig. 5. This system provides a 2.15 MHz Larmor frequency and allows imaging with resolution on the scale of 2–3 mm. While in many ways a system such as this will not be competitive to contemporary in vivo clinical imaging systems, the combination of much lower initial cost, lower infrastructure and maintenance costs may well make such a system compelling, especially for use in regions where conventional clinical imaging systems are not available.

Most of these permanent magnet systems produce Larmor frequencies in the radio-frequency regime and require rf electronics consoles. While a number of vendors supply low-cost and portable spectrometer consoles suitable for these applications, these products remain expensive enough to be lab instruments beyond the reach of enthusiasts. However, a number of groups have demonstrated both low-field and rf NMR spectrometer electronics that can be constructed inexpensively from readily available parts. The availability of high-performance FPGA devices has allowed the home builder to produce rf systems competitive with the most sophisticated commercial offerings. The OPENCORE NMR system [46] for example has provided the building blocks to produce a digital rf system based on an Altera Cyclone II FPGA.

Perhaps more exciting however, is the recent entry to the marketplace of inexpensive software-defined radio devices. Targetted primarily for wireless communications systems, full-duplex software-defined radios produce programmable streams of rf output and can receive and demodulate rf input. While these systems are most often connected to antennas for transmitting and receiving communications signals like digital radio, television, networking, and global positioning, their capabilities are generally well aligned with the needs of an NMR console. An early SDR-based NMR system [47] demonstrated the promise of this SDR approach, but required fabrication of sophisticated electronics to implement. Since then, commercially available, but "mass-market" devices have become available. An MRI system was built using the open source GNU radio platform and USRP (Ettus Research, Santa Clara, CA) SDR hardware [48]. The use of a low-cost SDR hardware device significantly lowers the barrier to adoption compared with designs requiring fabrication of high-speed rf printed circuit boards.

Another significant step in affordability has come with the introduction of "crowd-sourced" SDR devices such as the LimeSDR, which is a complete USB-connected SDR aimed at the hacker/DIY market. This device has been used both in our lab [49] and elsewhere [50]. Our work showed that multiple LimeSDR boards could be combined and synchronized to make a multi-channel, multi-nuclear NMR spectrometer, competitive with the state-of-the art from the large commercial vendors, at a tiny fraction of the cost of the commercial offerings. The level of integration on this board is sufficient that simple NMR spectra can be collected with a low-power rf transmit/receive switch as the only external component between the LimeSDR and the NMR probe. With external power amplifiers and pre-amplifiers, a complete NMR console can be assembled. The fast ADCs and DACs on this system allow spectral widths as high as 50 MHz (Figs. 6a and 6b). Able to tune frequencies from near dc to several GHz, devices like this promise to revolutionize the availability of NMR electronics. To accompany the rf system of the LimeSDR, we developed firmware for the widely-available arduino Due microcontroller board to allow it to function as a general purpose digital pulse programmer, used to control gating, amplifier blanking, and other accessories.

A different approach was used by Doll [50], who modified the LimeSDR's FPGA firmware to allow its onboard GPIO pins to be used in real-time, synchronized with the rf. That work used the LimeSDR not only for pulsed NMR, but also pulsed and cw EPR, shown in Figs. 6c–6e.

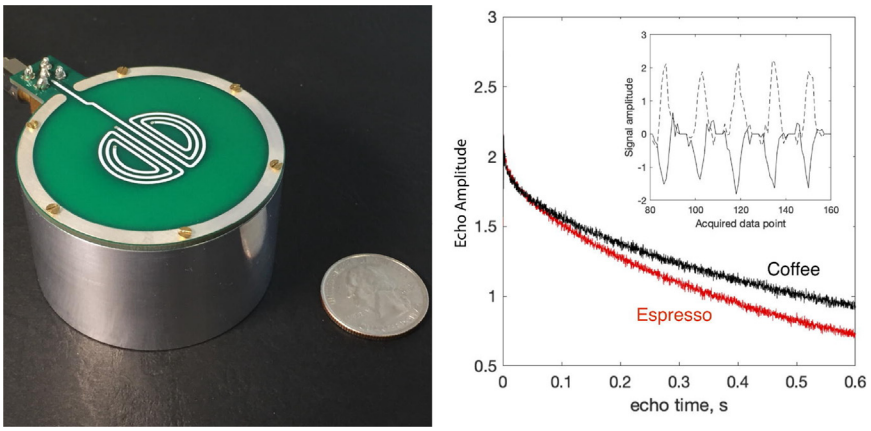

Fig. 3. (Left) A small sensor built with a barrel magnet and integrated rf coil. (Right) CPMG signals obtained using the barrel magnet sensor from a coffee (black) and an espresso (red) drink. The inset is the 6–10th echoes after 2 scans. The echo spacing is 250 μs. Reprinted from Ref. [41], Copyright 2019, with permission from Elsevier. (For interpretation of the references to color in this figure legend, the reader is referred to the web version of this article.)

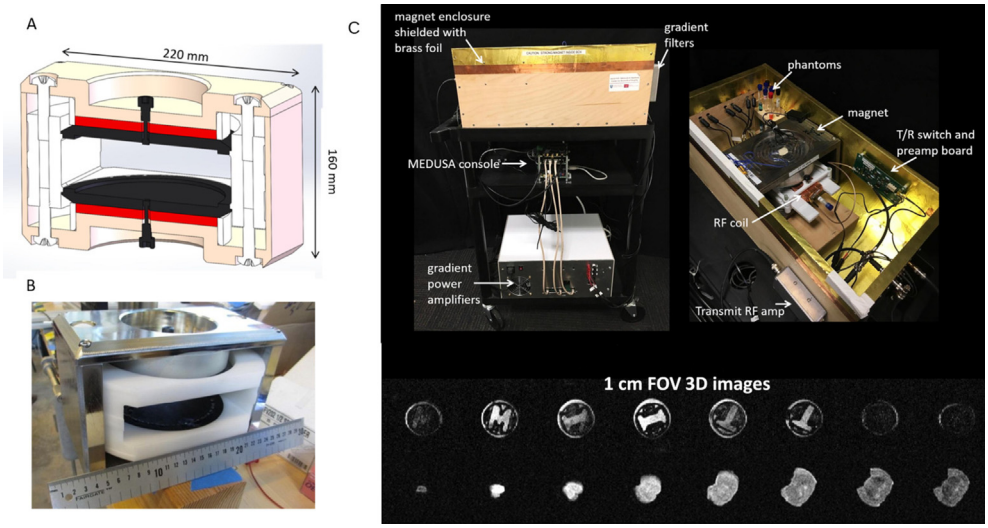

Fig. 4. (A) and (B) NdFeB H-yoke magnet built for low-cost table top educational imaging system. The 13 kg magnet assembly produces an 0.18 T B_0 with 50 ppm homogeneity over a 1 cm diameter spherical region. (C) Photos of the complete tabletop system including rf console and gradient power supplies along with 3D RARE images of a 3D printed "M-I-T" phantom and a mouse brain. See original article for details. Reprinted from Ref. [42], Copyright 2019, with permission from Elsevier.

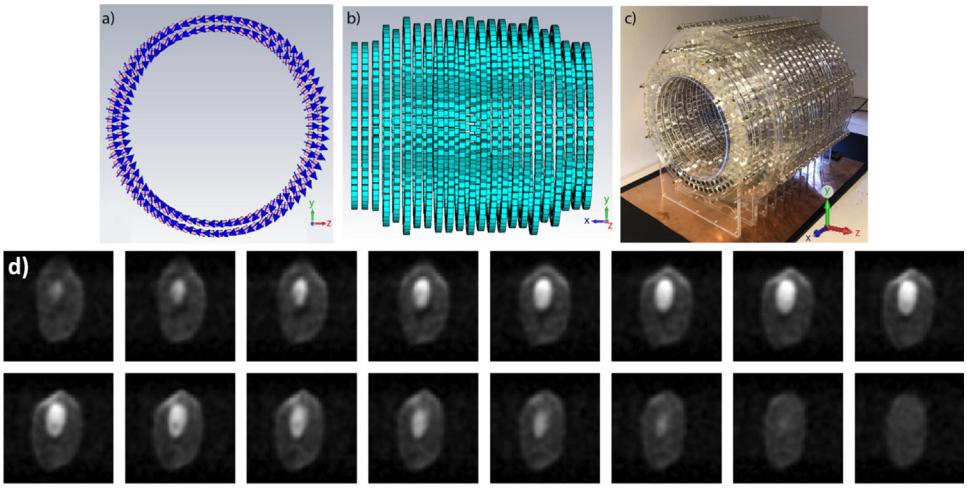

Fig. 5. Halbach magnet array for pediatric imaging. (a) The array is constructed from two layers of magnet elements organized in 23 rings. (b) A side view shows the variation in diameter of the rings in order to optimise homogeneity. (c) The final constructed array. Each ring was constructed separately using a PMMA holder fixed together using threaded brass rods. (d) Slices from a T1-weighted 3D image data set of an "avocado in watermelon" head phantom. Reprinted from Ref. [45], Copyright 2019, with permission from Elsevier.

Both of these approaches relied on the fact that the LimeSDR is a completely open-source project, where not only the software libraries used to access the device are available and modifiable, but the source for the FPGA "gateware" is published and licensed so that it can be freely modified and redistributed. This open-source development model has also made important impacts on some of the instrumentation used in hardware development. An example here is the NanoVNA project [51], which has brought the cost of a network analyzer, essential in the development of many rf circuits, down by orders of magnitude, to below $100.

4. An ultra low-cost system applied to inhomogeneous magnetization transfer

While the LimeSDR and, presumably future SDR devices appear to cover the console electronics needs at radio-frequencies, the digital rf techniques used in these sorts of systems can be applied at low frequency at even lower cost. As a demonstration of what is possible at low field outside of the lab environment, we now discuss a simple low-field NMR spectrometer system assembled in the midst of the lock-down response to the spring of 2020 COVID-19 pandemic.

We have assembled a modest NMR spectrometer to work at frequencies up to $\sim$ 200 kHz. This system is based upon an arduino Due microcontroller that offers significant performance enhancements over the Uno used in [30]. While significantly more powerful microcontrollers are available, the Due has a number of advantages, including its availability from numerous vendors as well as software support in the widely available and easy-to-use arduino programming environment [52]. This system is powerful enough to allow for fully digital rf transmit and receive methods similar to those used in SDR and commercial NMR systems, though at much lower frequency.

The onboard DACs on the Due allow the microcontroller to produce true sinusoidal outputs. In the configuration used here, one DAC output produces the rf signal and the second is available, for example using an external analog multiplier chip, for amplitude

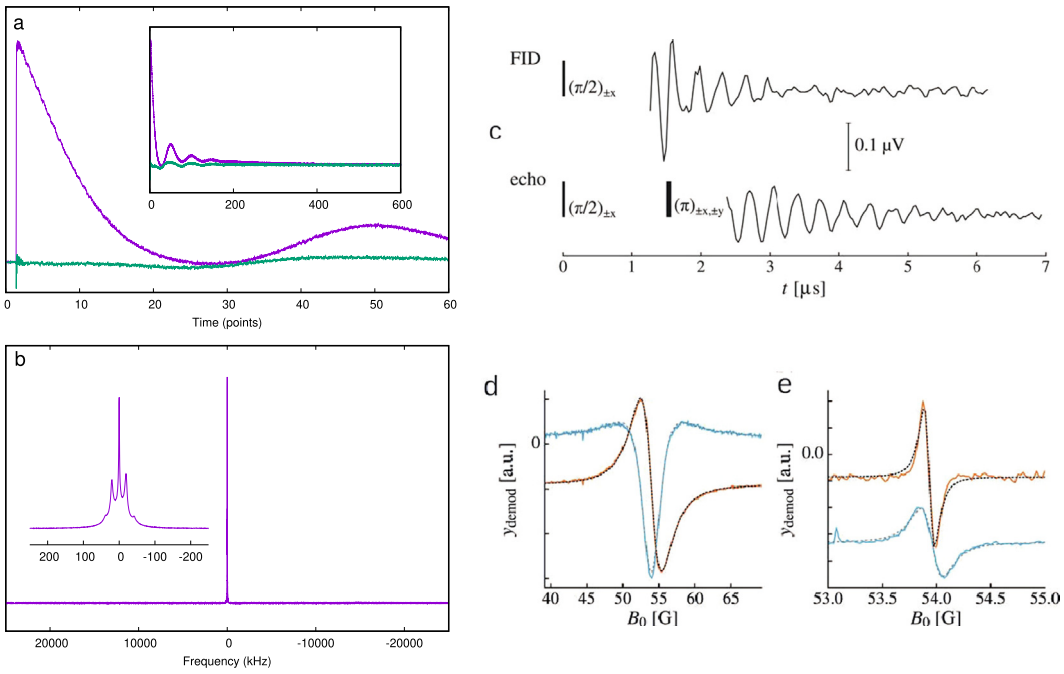

Fig. 6. The LimeSDR crowd-sourced software-defined radio board as a high performance magnetic resonance transceiver. (a) and (b) show the fid and spectrum of ^{1}H in $CaSO_4 \cdot \frac{1}{2}H_2O$, acquired with a spectral width of 50 MHz. The ∼100 kHz wide Pake pattern shown in the inset of (b) appears as a sharp peak when the entire spectral width is displayed. (c) Real part of the ESR FID and echo at 149.4 MHz from a degassed trityl radical solution. CW EPR of (d) Lithium phthalocyanine and (e) a 500 μM solution of trityl radical. (a) and (b) reprinted from Ref. [49], Copyright 2018 Wiley Periodicals, Inc, used with permission. (c)–(e) reprinted from Ref. [50], Copyright 2019 A. Doll. Licensed under a Creative Commons Attribution (CC BY) license (http://creativecommons.org/licenses/by/4.0/).

modulation. Alternatively configuring the two DACs to produce quadrature outputs for orthogonal excitation coils would be straightforward. In the present implementation, both the DAC and 12-bit ADC used for signal acquisition are operated at a fixed rate of 500,000 samples per second. Down-converting, quadrature detection, digital filtering and downsampling are done on board resulting in the microcontroller delivering 15-bit resolution in-phase and quadrature samples at 20 ksps. The microcontroller interprets pulse programs that control the rf output, its phase, and up to 26 digital outputs. A small code library has been written to facilitate generating pulse programs and communications and control the device. The external circuitry required to collect NMR spectra with this device consists of three op-amps, two switches (reed relays were used here) and a handful of resistors, capacitors, and diodes. Preliminary measurements were collected at 63.6 kHz in the magnetic field produced by the crudely hand-wound coil that was originally used as the polarization coil for our Earth's field work [30]. This coil consists of three layers of 125 turns of 18 AWG copper wire wound on a 15 cm long section of 4" ABS plastic drain-waste-vent pipe. The coil was not designed with homogeneity in mind, and the spectral linewidth is on the order of 1.5% of the Larmor frequency, though it is likely this could be improved substantially with the addition of additional end windings. The coil used for transmit and receive is two layers of 150 turns/layer of 30-AWG wire wound on a 2" PVC pipe. This coil was wound for an unrelated project and again was not designed specifically for the task at hand; due to the constraints of the lock-down, it was the best coil available. The amplifier used for transmit is a simple LF411 op-amp. Connecting the op-amp, with a gain of 11, yields a 22 Vpp output that provides a B_1 strength of about 700 Hz. Inserting a 470 pF capacitor in series with the coil provides a Q of approximately 9, increasing B_1 to more than 6 kHz. The voltage across the coil in this configuration reaches nearly 220 Vpp. With this capacitor inserted however, pulses are far from rectangular because the ring-up and ring-down time of the circuit (∼ 160 μs) is longer than the nominal duration of a $\pi/2$ or π pulse. For most of the measurements below this series capacitor was omitted.

During signal reception, the coil is tuned with a parallel 470 pF capacitor. The receiver itself is composed of two LT1007 op-amp amplification stages with a total gain of about 5100. The received signals are both low pass filtered (130 kHz) and high pass filtered (17 kHz) and level-shifted so the signals' dc level is near the center of the Due's 0–3.3 V ADC input range. More aggressive filtering of the analog signals is not required as the Due provides digital filtering with a bandwidth of about 5 kHz. The entire "console" consists of an arduino Due and the transmit and receive amplifiers assembled on a 5x16 cm solderless breadboard, and has a total parts cost of perhaps $30 (not including coils and power supplies). A diagram of the entire apparatus is shown in Fig. 7B.

The magnet coil is supplied with 1.76 A from a bench supply (Circuit Test PSB-3030) with a large (150 mF) capacitor in parallel to remove some of the supply's output noise, but otherwise unstabilized. Because the B_0 homogeneity is relatively poor in this magnet, a CPMG sequence was used for all measurements.

The intention for this system is to add to our recent efforts to understand the physics underlying a technique known as inhomogeneous magnetization transfer [53] which was introduced in 2015 as a technique to map myelin in vivo [54]. In this technique magnetization transfer pre-pulses are applied to the patient at a frequency offset from the water resonance but within the width of the dipole-coupling broadened lines of the semi-solid tissue components. This partial saturation of the semi-solids is transferred to the water by chemical exchange or cross-relaxation where it can be detected as a decrease in the intensity of the water signal. It was found that for lamellar lipid systems the amount of saturation was significantly higher if prepulses were applied simultaneously (or interleaved) at both positive and negative frequency offsets compared to single-sided pre-pulses of the same rf power.

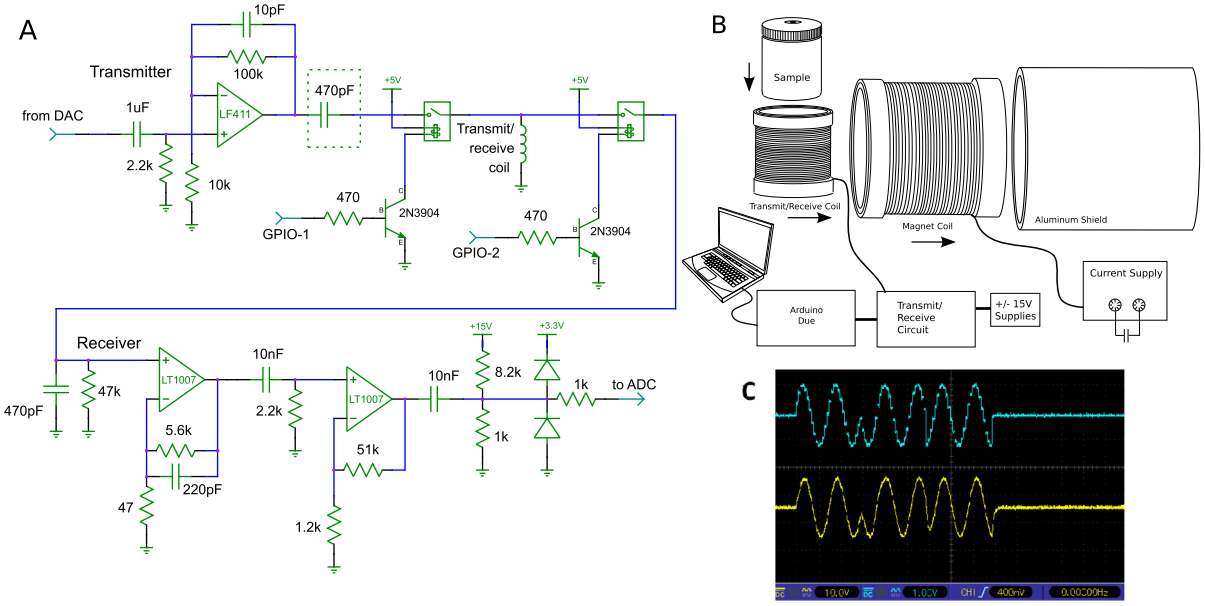

Fig. 7. Arduino Due based low-field NMR spectrometer. (A) shows the circuit diagram for the transmit and receive circuitry not provided by the microcontroller. The 470 pF capacitor in the dashed box can be used to create a series resonance while the transmitter is active, resulting in a significantly higher B_1, or removed to create weaker pulses with no ring-up or ring-down. (B) is a block diagram of the complete system. Connections between the Due and the transmit/receive circuit include the DAC output, ADC input, two digital logic lines to control relays, +5 and +3.3 V supplies. (C) is an oscilloscope capture of the rf output at 33.6 kHz in which two phase shifts, of 180 and 90° can be observed. The upper trace comes directly from the microcontroller where the 2 μs sample frequency can be observed. The lower trace is the output of the transmitter amplifier which incorporates a low-pass anti-aliasing filter.

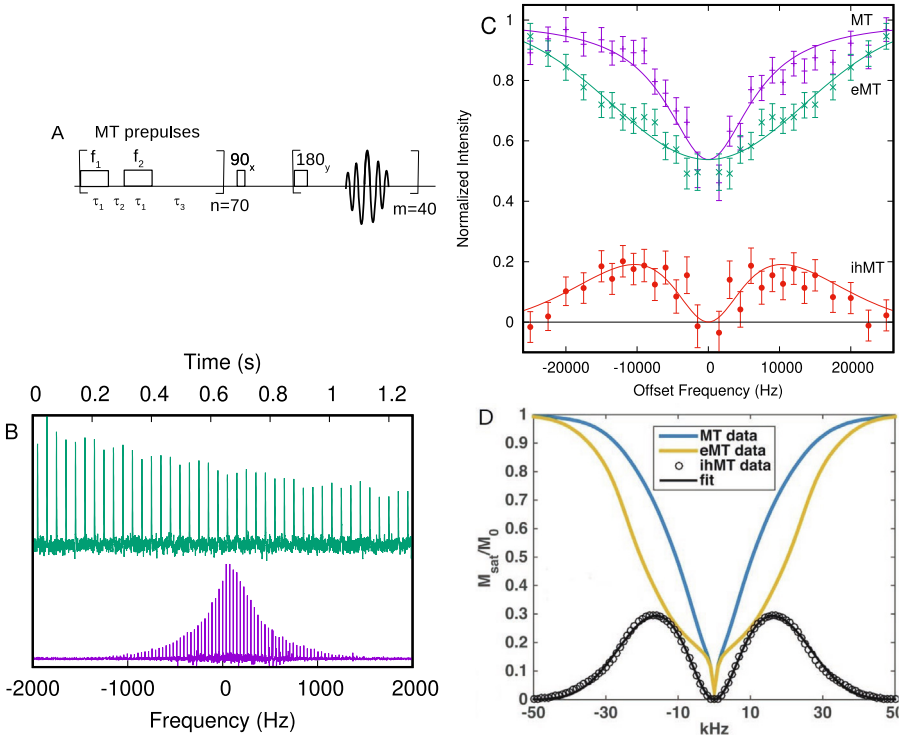

Fig. 8. Low-field ihMT experiments. (A) ihMT-CPMG pulse sequence. For single-sided MT experients, $f_1 = f_2$. For dual-irradiation experiment $f_1 = -f_2$. Experiments here were performed with τ_1 = 2 ms, τ_2 = 1 ms and τ_3 = 5 ms. (B) NMR echo data from the Due-based spectrometer at 63.6 kHz. The top trace shows a train of 40 echoes with 32 ms echo spacing. The lower trace shows the Fourier transform of the echo train. (C) The signal intensity of a hair conditioner sample following magnetization transfer prepulses ($f_1 = f_2$), dual-frequency prepulses ($f_1 = -f_2$) and ihMTR. All signals normalized for direct excitation of the water signal. The signal suppression of the MT data were fitted to a Lorentzian lineshape, eMT data were fitted to a Gaussian lineshape and ihMT to the difference. (D) shows MT, eMT and ihMT from a lamellar lipid sample at 500 MHz. (D) reprinted from Ref. [55], Copyright 2016, Wiley Periodicals, Inc, used with permission.

An important parameter in this effect is T_{1D}, the dipolar relaxation time, which must be sufficiently long. A figure of merit, ihMTR has been defined as

$$\text{ihMTR} = \frac{S_+ + S_- - 2S_{\text{dual}}}{2S_0}, \quad (5)$$

in which S_+ is the signal intensity following prepulses at positive offsets, S_- it the signal with prepulses at negative offsets, S_{dual} is the signal with prepulses at both positive and negative offsets, and S_0 is the signal with no prepulses. It has been found that ihMTR correlates with the abundance of myelin in brain [54].

It is well known that T_1 contrast can be significantly enhanced in vivo at low field where the Zeeman and dipolar interactions become comparable in size [56,57]. With the low-field spectrometer in its current condition, we have begun to explore magnetization transfer (MT) and the ihMT in a white-matter brain tissue phantom (hair conditioner). Measurements of the dependence of MT and ihMT on prepulse offset frequency are shown in Fig. 8A. The prepulse train used here consists of 70 pairs of pulses over 700 ms, as shown in Fig. 8B. These preliminary, unoptimized results bear a striking resemblance to data collected at 500 MHz [55], shown in Fig. 8D and suggest that the study of these promising effects will be feasible at very low field with inexpensive hardware. To our knowledge, these are the first ihMT experiments in this frequency regime, and were made in a home during the COVID-19 isolation/quarantine period in the spring of 2020. It will be interesting to study the field dependence of these effects, especially in a regime where the dipolar coupling strength and Zeeman interactions are of similar size.

Enhancements planned for this system include (1) a purpose-designed transmit/receive coil with either a similar number of turns and a greater wire size or wound with Litz wire (2) solid-state transmit/receive switching, and (3) a magnet with improved homogeneity, which will allow a dramatic increase in sensitivity. The circuit schematics, arduino Due firmware, support library, and pulse program used to collect the above ihMT data have been published under an open-source license and are available for download at http://www.phas.ubc.ca/%7Emichal/Due-nmr.

5. Conclusions

While NMR is commonly thought of as an expensive technique requiring large institutional investment, many applications at low and modest magnetic field are possible with inexpensive, easily constructed equipment. Potential applications for NMR in industry abound, and we have touched on only a handful of the many examples that have been described in the literature. The availability of powerful and easy-to-use electronic devices like microcontrollers, FPGAs, and SDRs has reduced the cost of the transmit and receive electronics to the point where they are accessible to hobbyists, and no longer limit access to dedicated laboratories. While industrial and educational applications are important beneficiaries of these developments, substantial science is possible with very low-cost equipment, as is demonstrated by ihMT results presented here. The similarity of our results at 63 kHz to those at 500 MHz is striking. The inexpensive instrument will also allow access to even lower frequencies where additional phenomena, which cannot be easily studied at high field, are likely to be important.

Declaration of Competing Interest

The authors declare that they have no known competing financial interests or personal relationships that could have appeared to influence the work reported in this paper.

Acknowledgements

This work was supported by a Discovery Grant from the Natural Sciences and Engineering Research Council of Canada. The author thanks Stefan Reinsberg and Luke Reynolds for comments on a draft of the manuscript and Mark Conradi for a helpful discussion on shielding.

References

[1] D.I. Hoult, R.E. Richards, The signal-to-noise ratio of the nuclear magnetic resonance experiment, J. Magn. Reson. 24 (1976) 71–85, https://doi.org/10.1016/0022-2364(76)90233-X.
[2] D.I. Hoult, The NMR receiver: a description and analysis of design, Prog. NMR Spectrosc. 12 (1978) 41–77, https://doi.org/10.1016/0079-6565(78)80002-8.
[3] G. Brisebois, Op amp selection guide for optimum noise performance (2005). URL https://www.analog.com/media/en/reference-design-documentation/design-notes/dn355f.pdf.
[4] P. Lee, Low noise amplifier selection guide for optimal noise performance (2012). URL https://www.analog.com/media/en/technical-documentation/application-notes/an-940.pdf.
[5] M.S. Conradi, A.P. Zens, RF shielding and eddy currents in NMR probes, J. Magn. Reson. 305 (2019) 180–184, https://doi.org/10.1016/j.jmr.2019.06.011.
[6] S. Fahy, C. Kittel, S.G. Louie, Electromagnetic screening by metals, Am. J. Phys. 56 (1988) 989–992, https://doi.org/10.1119/1.15353.
[7] M.S. Conradi, S.A. Altobelli, N.J. Sowko, S.H. Conradi, E. Fukushima, Pre-polarization fields for Earth's field NMR: Fast discharge for use with short t_1 and large coils, J. Magn. Reson. 281 (2017) 241–245, https://doi.org/10.1016/j.jmr.2017.06.001.
[8] B.F. Melton, V.L. Pollak, Instrumentation for the Earth's field NMR technique, Rev. Sci. Instrum. 42 (1971) 760–773, https://doi.org/10.1063/1.1685227.
[9] A. Mohorič, G. Planinšič, M. Kos, A. Duh, J. Stepišnik, Magnetic resonance imaging system based on earth's magnetic field, Instrument. Sci. Technol. 32 (2004) 655–667, https://doi.org/10.1081/CI-200037034.
[10] P. Mahravarkar, S. Singh, S. Labde, V. Dongre, A. Patil, The low cost proton precession magnetometer developed at the Indian Institue of Geomagnetism, J. Inst. 12 (2017) T05002, https://doi.org/10.1088/1748-0221/12/05/T05002.
[11] S. Appelt, F.W. Haesing, S. Baer-Lang, N.J. Shah, B. Blümich, Proton magnetization enhancement of solvents with hyperpolarized xenon in very low-magnetic fields, Chem. Phys. Lett. 348 (2001) 263–269, https://doi.org/10.1016/S0009-2614(01)01106-X.
[12] M.E. Halse, P.T. Callaghan, A dynamic nuclear polarization strategy for multi-dimensional Earth's field NMR spectroscopy, J. Magn. Reson. 195 (2008) 162–168, https://doi.org/10.1016/j.jmr.2008.09.007.
[13] P.M. Richardson, A.J. Parrott, O. Semenova, A. Nordon, S.B. Duckett, M.E. Halse, SABRE hyperpolarization enables high-sensitivity a ^{1}h and ^{13}c benchtop NMR spectroscopy, Analyst 143 (2018) 3442–3450, https://doi.org/10.1039/C8AN00596F.
[14] B. Blümich, Low-field and benchtop NMR, J. Magn. Reson. 306 (2019) 27–35, https://doi.org/10.1016/j.jmr.2019.07.030.
[15] B. Blümich, C. Rehorn, W. Zia, Magnets for Small-Scale and Portable NMR in Advanced Micro and Nanosystems, Wiley, 2018, pp. 1–20. doi:10.1002/9783527697281.ch1 (Chapter 1).
[16] C. Snow, R.L. Driscoll, A compensated solenoid giving a uniform magnetic field over a large volume, J. Res. Natl. Bureau Stand. C 69C (1965) 49–54, https://doi.org/10.6028/jres.069C.009.
[17] I. Sasada, Y. Nakashima, Planar coil system consisting of three coil pairs for producing a uniform magnetic field, J. Appl. Phys. 99 (2006) 08D904, https://doi.org/10.1063/1.2165107.
[18] C.P. Bidinosti, J. Choukeife, P.-J. Nacher, G. Tastevin, In vivo NMR of hyperpolarized ^{3}He in the human lung at very low magnetic fields, J. Magn. Reson. 162 (2003) 122–132, https://doi.org/10.1016/S1090-7807(02)00198-2.
[19] M. Packard, R. Varian, Free nuclear induction in the earth's magnetic field, Phys. Rev. 93 (1954) 941.
[20] S. Hollos, R. Hollos, Signals From the Subatomic World: How to Build a Proton Precession Magnetometer, Abrazol Publishing, Longmont, CO, 2008.
[21] B. Worley, PyPPM: A proton precession magnetometer for all. URL https://github.com/geekysuavo/pyppm (accessed July 21, 2020).
[22] D. Duret, J.M. Leger, M. Frances, J. Bonzom, F. Alcouffe, A. Perret, J.C. Llorens, C. Baby, Performances of the ovh magnetometer for the danish oersted satellite, IEEE Trans. Magn. 32 (1996) 4935–4937, https://doi.org/10.1109/20.539293.
[23] Teachspin web site. URL https://www.teachspin.com/earths-field-nmr (accessed June 8, 2020)
[24] P. Jansen, Low-field MRI continued. URL https://hackaday.io/project/12352-low-field-mri-continued (accessed June 23, 2020).
[25] G.J. Béné, Nuclear magnetism of liquid systems in the earth field range, Phys. Rept. 58 (1980) 213–267, https://doi.org/10.1016/0370-1573(80)90012-5.
[26] J. Stepišnik, V. Eržen, M. Kos, NMR imaging in the earth's magnetic field, Magn. Reson. Med. 15 (1990) 386–391, https://doi.org/10.1002/mrm.1910150305.
[27] P.T. Callaghan, C.D. Eccles, J.D. Seymour, An earth's field nuclear magnetic resonance apparatus suitable for pulsed gradient spin echo measurements of self-diffusion under antarctic conditions, Rev. Sci. Instrum. 68 (1997) 4263–4270, https://doi.org/10.1063/1.1148340.

[28] H.K.S. Appelt, W. Häsing, B. Blümich, Chemical analysis by ultra high-resolution nuclear magnetic resonance in eht Earth's magnetic field, Nat. Phys. 2 (2006) 105–109, https://doi.org/10.1038/nphys211.
[29] M.S. Conradi, S.A. Altobelli, N.J. Sowko, S.H. Conradi, E. Fukushima, Earth's field NMR detection of oil under arctic ice-water suppression, J. Magn. Reson. 288 (2018) 95–99, https://doi.org/10.1016/j.jmr.2018.02.004.
[30] C.A. Michal, A low-cost spectrometer for NMR measurements in the Earth's magnetic field, Meas. Sci. Technol. 21 (2010) 105902, https://doi.org/10.1088/0957-0233/21/10/105902.
[31] C.A. Michal, Magnetic resonance imaging in the first year lab, Phys. Canada 70 (2014) 120–122.
[32] J. Pommier, H. Benoit, Nonlinear effects in an NMR experiment, IEEE J Quant. Elec. QE-2 (1966) 388–390, https://doi.org/10.1109/JQE.1966.1074071.
[33] P.T. Eles, C.A. Michal, Two-photon excitation in nuclear magnetic and quadrupole resonance, Proc. Nucl. Magn. Reson. Spect. 56 (2010) 232–246, https://doi.org/10.1016/j.pnmrs.2009.12.002.
[34] M.E. Halse, P.T. Callaghan, Terrestrial magnetic field NMR: recent advances, eMagRes (2009), https://doi.org/10.1002/9780470034590.emrstm1025.
[35] P.F. de J. Cano-Barrita, A.E. Marble, B.J. Balcom, J.C. Garcia, I.V. Masthikin, M.D. A. Thomas, T.W. Bremner, Embedded NMR sensors to monitor evaporable water loss caused by hydration and dring in portland cement mortar, Cem. Concr. Res. 39 (2009) 324–328, https://doi.org/10.1016/j.cemconres.2009.01.011.
[36] B. Blümich, J. Perlo, F. Casanova, Mobile single-sided NMR, J. Magn. Reson. 52 (2008) 197–269, https://doi.org/10.1016/j.pnmrs.2007.10.002.
[37] E.D. Federico, S.A. Centeno, C. Kehlet, P. Currier, D. Stockman, A. Jershow, Unilateral NMR applied to the conservation of works of art, Anal. Bioanal. Chem. 396 (2009) 213–220, https://doi.org/10.1007/s00216-009-3128-7.
[38] B. Blümich, F. Casanova, J. Perlo, F. Presciutti, C. Anselmi, B. Doherty, Noninvasive testing of art and cultural heritage by mobile NMR, Acc. Chem. Res. 43 (2010) 761–770, https://doi.org/10.1021/ar900277h.
[39] M.N. Martin, B.J. Balcom, M.J. McCarthy, M.P. Augustine, Noninvasive, nondestructive measurement of tomato concentrate spoilage in large-volume aseptic packages, Food Eng. Mater. Sci. Nanotechnol. 84 (2019) 2898–2906, https://doi.org/10.1111/1750-3841.14778.
[40] R.H. Morris, M.I. Newton, P.R. Knowles, M. Bencsik, P.A. Davies, P. Griffin, G. McHale, Analysis of clogging in constructed wetlands using magnetic resonance, Analyst 136 (2011) 2283–2286, https://doi.org/10.1039/C0AN00986E.
[41] Y.-Q. Song, S. Utsuzawa, Y. Tang, Low fields but high impact: Ex-situ NMR and MRI, J. Magn. Reson. 306 (2019) 109–111, https://doi.org/10.1016/j.jmr.2019.07.026.
[42] C.Z. Cooley, J.P. Stockmann, T. Witzel, C. LaPierre, A. Mareyam, F. Jia, M. Zaitsev, Y. Wenhui, P. Stang, G. Scott, E. Adalsteinsson, J.K. White, L.L. Wald, Design and implementation of a low-cost, tabletop MRI scanner for education and research prototyping, J. Magn. Reson. 310 (2019) 106625, https://doi.org/10.1016/j.jmr.2019.106625.
[43] P.P. Stang, S.M. Conolly, J.M. Santos, J.M. Pauly, G.C. Scott, Medusa: A scalable MR console using USB, IEEE Trans. Med. Imag. 31 (2012) 370–379, https://doi.org/10.1109/TMI.2011.2169681.
[44] C.A. Michal, K. Broughton, E. Hansen, A high performance digital receiver for home-built nuclear magnetic resonance spectrometers, Rev. Sci. Instrum. 73 (2002) 453–458, https://doi.org/10.1063/1.1433950.
[45] T. O'Reilly, W.M. Teeuwisse, A.G. Webb, Three-dimensional MRI in a homogenous 27 cm diameter bore Halbach array magnet, J. Magn. Reson. 307 (2019) 106578, https://doi.org/10.1016/j.jmr.2019.106578.
[46] K. Takeda, OPENCORE NMR: open-source core modules for implementing an integrated FPGA-based NMR spectrometer, J. Magn. Reson. 192 (2008) 218–229, https://doi.org/10.1016/j.jmr.2008.02.019.
[47] W. Tang, W. Wang, A single-board NMR spectrometer based on a software defined radio architecture, Meas. Sci. Technol. 22 (2011) 015902, https://doi.org/10.1088/0957-0233/22/1/015902.
[48] C.J. Hasselwander, Z. Cao, W.A. Grissom, gr-MRI: A software package for magnetic resonance imaging using software defined radios, J. Magn. Reson. 270 (2016) 47–55, https://doi.org/10.1016/j.jmr.2016.06.023.
[49] C.A. Michal, A low-cost multi-channel software-defined radio-based NMR spectrometer and ultra-affordable digital pulse programmer, Concepts Magn. Reson. Part B (2018) e21401, https://doi.org/10.1002/cmr.b.21401.
[50] A. Doll, Pulsed and continuous-wave magnetic resonance spectroscopy using a low-cost software-defined radio, AIP Adv. 9 (2019) 115110, https://doi.org/10.1063/1.5127746.
[51] Nanovna. URL https://nanovna.com (accessed June 28, 2020).
[52] The Arduino homepage. URL https://www.arduino.cc (accessed June 12, 2018).
[53] A.P. Manning, K.L. Chang, A.L. MacKay, C.A. Michal, The physical mechanism of inhomogeneous magnetization transfer MRI, J. Magn. Reson. 274 (2017) 125–136, https://doi.org/10.1016/j.jmr.2016.11.013.
[54] G. Varma, G. Duhamel, C. de Bazelaire, D. Alsop, Magnetization transfer from inhomogeneously broadened lines: a potential marker for myelin, Magn. Reson. Med. 73 (2015) 614–622, https://doi.org/10.1002/mrm.25174.
[55] S.D. Swanson, D.I. Malyarenko, M.L. Fabilli, R.C. Welsh, J.-F. Nielsen, A. Srinivasan, Molecular, dynamic, and structural origin of inhomogeneous magnetization transfer in lipid membranes, Magn. Reson. Med. 77 (2017) 1318–1328, https://doi.org/10.1002/mrm.26210.
[56] R.D. Brown III, S.H. Koenig, $1/T_{1\rho}$ and low-field $1/T_1$ of tissue water protons arise from magnetization transfer to macromolecular solid-state broadened lines, Magn. Reson. Med. (1992) 145–152, https://doi.org/10.1002/mrm.1910280115.
[57] S.K. Lee, M. Möβle, W. Myers, N. Kelson, A.H. Trabesinger, A. Pines, J. Clarke, Squid-detected MRI at 132 μT with T_1-weighted contrast established at 10 μ T-300 mT, Magn. Reson. Med. 53 (2005) 9–14. https://doi.org/10.1002/mrm.20316.